Low-order harmonic generation in metal ablation plasmas in nanosecond and picosecond laser regimes

M. López-Arias[a,b], M. Oujja[a], M. Sanz[a], R. A. Ganeev[c], G. S. Boltaev[c], N. Kh. Satlikov[c], R. I. Tugushev[c], T. Usmanov[c], and M. Castillejo[a,*]

[a]*Instituto de Química Física Rocasolano, CSIC, Serrano 119, 28006 Madrid, Spain.*

[b]*Unidad Asociada Departamento de Química Física I, Facultad de Ciencias Químicas, Universidad Complutense de Madrid, 28040 Madrid, and Instituto de Estructura de la Materia, CSIC, Serrano 123, 28006 Madrid, Spain.*

[c]*Institute of Electronics, Uzbekistan Academy of Sciences, Akademgorodok, 33, Dormon Yoli Street, Tashkent 100125, Uzbekistan.*

[*]*E-mail:* marta.castillejo@iqfr.csic.es

Abstract

Low-order harmonics, 3rd and 5th, of IR (1064 nm) laser emission have been produced in laser ablation plasmas of the metals manganese, copper and silver. The harmonics were generated in a process triggered by laser ablation followed by frequency up-conversion of a fundamental laser beam that propagates parallel to the target surface. These studies were carried out in two temporal regimes by creating the ablation plasma using either nanosecond or picosecond pulses and then probing the plasma plume with pulses of the same duration. The spatiotemporal behaviour of the generated harmonics was characterized and reveals the distinct composition and dynamics of the plasma species that act as nonlinear media, allowing the comparison of different processes that control the generation efficiency. These results serve to guide the choice of laser ablation plasmas to be used for efficient high harmonic generation of laser radiation.

I INTRODUCTION

Harmonic generation (HG) of intense laser pulses in isotropic media such as gases and vapours serves to create coherent radiation in the short wavelength range of the spectrum down to the extreme ultraviolet (XUV) and X-ray regions. Low-order frequency up conversion using laser pulses of nanosecond (ns) duration have provided table-top vacuum ultraviolet (VUV) coherent light for spectroscopy and molecular photodissociation studies.[1,2] On the other hand, high-order harmonic generation[3] (HHG) requires pulses of higher intensities (typically 10^{14}-10^{15} W/cm^2) which can easily be achieved with femtosecond (fs) driving lasers. Although the phenomenon of HG is universal and can be generalized to any material with sufficient non linear response, mostly atomic,[4,5] or in some cases, molecular[6,7] gas jets have been investigated as non-linear media. In practical applications of coherent short wavelength HG sources, a high conversion efficiency and thus high photon flux of the harmonic radiation are essential.

Since the beginning of the nineties, ions generated in laser ablation plasmas have been investigated as alternative isotropic media for HHG.[8-12] The higher ionization potentials of ions as compared with neutral noble gas atoms would result in the extension of the harmonic cutoff towards shorter wavelengths. However, those experiments have shown that ionization-induced defocusing of the fundamental laser beam plays a detrimental effect on the HHG process.

Together with atomic ions and neutrals, laser ablation can easily generate other species, such as aggregates, clusters and nanoparticles, with various nonlinear optical properties and a relative abundance that can in principle be controlled by the right choice of solid target and laser wavelength and pulse duration. Akiyama *et al* [9] noted that control of limiting factors (self-defocusing and wave phase mismatch between the harmonics and the radiation being converted) leads to efficient HHG in alkali ions generated by laser

ablation. In the last few years more research has demonstrated the advantages of using various low-excited and weakly ionized ablation prepared plasmas for HHG.[13-15] These advantages concern, among others, the substantial increase of the generated highest harmonic order, the emergence of a plateau in the energy distribution of highest-order harmonics, the high HHG yield achieved with several plasma formations, the realization of resonance-induced enhancement of individual harmonics, the efficient harmonic enhancement for cluster containing plasma plumes, etc.

For understanding the impeding and restricting processes of HG in laser generated plasmas and identifying the media that lead to highly efficient up conversion, the analysis of low-order harmonics can be a clearly justified approach, since, for lowest orders, one can clearly define the processes which hamper further enhancement of conversion efficiency. Examples of this approach are recent investigations of low-order harmonic generation in ablation plumes of dielectric and semiconductor solid targets using Q-switched Nd:YAG lasers with pulses of ns duration.[16,17]

In this work we have investigated in two time domains, embracing the ns and picosecond (ps) scales low-order HG in ablation plasmas of the metals manganese (Z= 25), copper (Z= 29) and silver (Z=47), materials, which have already shown efficient nonlinear up conversion of laser wavelength into the UV and XUV ranges.[15,18] In the first case, two synchronized ns Q-switched Nd:YAG lasers emitting at 1064 nm were used for triggering the ablation event and as fundamental radiation for the HG process. In the second case, a ps Nd:YAG laser also operating at 1064 nm served both for ablation and as a source of fundamental radiation for frequency up conversion. Account will be given of the distinct spatial and temporal distribution of the harmonic signals across the plasmas, and of the differences observed between ns and ps regimes. The interest of this work relies on the capability of low-order HG to monitor *in situ* the

composition and dynamics of ablation plasma plumes and to define optimal schemes and plasmas, based in the widely used Nd:YAG lasers, for further development of coherent sources in the VUV near and below 200 nm range, a region where frequency doubling in non-linear crystals is extremely restricted.

II EXPERIMENTAL

Two setups were employed, corresponding to experiments in the ns and ps regimes. For HG with ns pulses,[16,17] ablation plasmas of manganese, copper and silver were generated in vacuum through normal incidence irradiation with a Q-switched Nd:YAG laser (Quantel, Brilliant B, 6 ns FWHM, 1064 nm) that was operated at 10 Hz using pulse energies of 2-35 mJ. This ablation beam was focused with a 17 cm focal length lens on the surface of the metal target down to a spot of 0.4 mm diameter (as measured by the print left on unplasticized polyvinyl chloride), generating maximum intensities of ~4.5×10^{9} W/cm^2, above the ablation thresholds. The vacuum chamber was kept at 10^{-2} mbar background pressure, and the samples were mounted on a rotating holder to avoid cratering. The harmonic driving IR fundamental radiation was delivered by a second Nd:YAG laser (Lotis TII LS-2147, 15 ns full-width-half-maximum, FWHM, 1064 nm, 10 Hz) propagating parallel to the target surface in such a way that it intersected the ablation plasma at a controllable distance from the surface (distances of 0.6 and 1 mm were employed). Typical pulse energies were in the range of 20-650 mJ. The beam was focused with a 20 cm focal length lens to a spot of 0.040 mm diameter, so that laser intensities in the harmonic generating region reached values of ~1.0×10^{11} - 3.5×10^{12} W/cm^2. The delay between this driving pulse and the ablation pulse was controlled electronically in the range from 0 to 10 μs.

Low-order harmonics of the driving laser were produced in the interaction region, and those propagated collinearly with the driving beam. Two highly IR transmissive, UV reflective mirrors were placed at the exit of the vacuum chamber to avoid damage of the detector with the intense IR beam. After the mirrors, a system consisting on a monochromator (TMc300 Bentham) with a ruled 300 lines/mm grating coupled to a time-gated, intensified charge-coupled-device (ICCD, 2151 Andor Technologies) was used for spectral discrimination and detection of the generated harmonics. For measurements, third (TH) and fifth (FH) harmonics were detected in the same spectral window by monitoring, together with the TH at 355 nm, the second order of the FH at 425.6 nm (2FH). Electronically excited species generated in the plasma produced optical emissions that could, under some conditions, be detected simultaneously with the harmonics. Typical acquisitions corresponded to an accumulation of 150 laser shots and a detection gate of 100 ns.

For HG with ps pulses, a home-made Nd:YAG laser operating at 1064 nm and delivering 38 ps pulses of up to 33 mJ at a 2 Hz pulse repetition rate was employed. The pulse was divided by a beam splitter in two beams, one used for ablating the target and the second as fundamental driving beam, conveniently delayed with respect to the former in the 15-50 ns range using an optical delay line. Typically, a 5 mJ pulse was focused down to a diameter of 0.5 mm by a 17 cm focal length lens on the targets for ablation. The driving beam, with energies per pulse of 0.5 to 28 mJ, was in turn focused by a 15 cm focal length lens to a focal spot of 0.030 mm diameter. The intensity of the ablating pulse on the target was 1.3×10^{11} W/cm^2, and that of the probe pulse ranged from 2.0×10^{12} to 1.0×10^{14} W/cm^2. The targets were ablated in vacuum and the up-converted radiation was measured by a fiber optic spectrometer HR4000 (Ocean Optics).

The metal targets employed in the experiments were purchased from E. Merck Darmstadt (Mn metal by electrolysis lumps) and Kurt Lesker (Ag, Cu 99.99 % purity).

III RESULTS AND DISCUSSION

Harmonics of the third and fifth orders (monitored at 355 nm and in second order of the grating at 425.6 nm respectively) of the fundamental 15 ns, 1064 nm beam were observed for each of the three metals in a range of ablation and probe laser energies and in a given spatiotemporal plume domain. Spontaneous emissions from excited species in the plume were recorded simultaneously with the signal from harmonics and consisted on the lines corresponding to atomic neutrals and ions. In the case of silver, some broad bands around 409 and 420 nm could also be attributed to AgO molecular emissions. As an example, Figure 1 gives proof of the TH and FH signatures for the case of copper when both ablation and fundamental beams were present. The second order of some atomic Cu emissions appears in the 430-440 nm region. Experiments performed with ablation and fundamental laser pulses of ps duration emitting at 1064 nm yielded efficient TH for the three metal plasmas. No signal was detected for the FH, because the spectral acquisition system in this case was based in a a fiber optic spectrometer with low efficiency at the corresponding wavelength.

Figure 2 shows for each of the three metals the behaviour of the TH as a function of the pulse energy of the ns ablation laser. The signal corresponding to the FH (not shown) closely follows that of the TH. In all cases, the onset of harmonic signal coincides with the appearance of a luminous plume, except for manganese, where harmonic signals were detected at pulse energies somehow lower than those necessary to observe the plume emission. Harmonic signals expectedly increase with ablation energy since this promotes the ejection of higher amount of material from the target and, thus, the higher

local densities of nonlinear emitters (through the expected quadratic dependence with local density[19]). As observed, maximum harmonic yield resulted at ablation pulse energies that increase with the atomic number of the metal, with values of 5, 10 and 12 mJ for Mn, Cu and Ag respectively. The decrease of the signal at higher pulse energies should be ascribed to the increase of free electron density in the plasma and their detrimental contribution to the phase mismatch. It is observed that when using ns ablation pulses, the Mn plasma can sustain HG in a wider range of ablation energies.

The nonlinear character of the emissions at 355 (TH) and 425.6 nm (2FH) was confirmed by studying the power dependence with respect to the pulse energy of the driving laser beam. Figure 3 displays those measurements for 6 ns, 1064 nm laser-generated plasmas of Mn, Cu and Ag when the driving laser was propagating at a distance of 0.6 mm from the surface. The slopes obtained in log-log plots were compatible in all three materials with the values of 3 and 5, expected for the behaviour of the TH and FH in the perturbative regime.

It should be noted that the relative intensity of the two spectral features displayed in Figure 3 for a given material does not directly reflect that of the generated harmonics because the spectra were not corrected by the response of the detection system. However, although no comparison is possible between two different harmonics generated in the plume of the same material, the yield of the same harmonic can be compared among the different materials. In fact, it is interesting to note that, in the range of fundamental beam pulse energies above 150 mJ (corresponding to an intensity of 7.9×10^{11} W/cm^2), the signal corresponding to the FH in the Mn plume, Figure 3(a), is higher than the corresponding signal in Cu and Ag plumes. This suggests that in the Mn ablation plume, FH generation could be enhanced, with respect to the other metals

studied, by a resonant effect due to the spectral proximity of a high oscillation strength transition.

As harmonic signal measurements displayed in Figure 3(a-c) were collected for each metal at ablation pulse energies corresponding to maximum up-conversion, i.e. 5, 10 and 12 mJ for Mn, Cu and Ag respectively, it is possible to establish a comparison between the harmonic generation efficiency in the plumes of the three metals studied. As indicated by the scales of the vertical axes in Figure 3(a-c) the highest and lowest TH yield are obtained for Mn and Ag respectively.

In the ps regime, the intensity of TH signal was also monitored as a function of the driving pulse energy. Due to the smaller range of registration of the fiber-optic-based acquisition system, the range of driving laser energies that could be explored in the ps regime was not as broad as in the experiments performed in the ns regime. Nevertheless the results are fully compatible with the expected cubic dependence. Also in the ps regime, Mn displayed the highest conversion efficiency.

The intensity of the emitted harmonics was sampled across the temporal-spatial region of the plume. This was done by monitoring on one hand the dependence with the delay between ablation and driving pulses, and on the other hand, with a set of *z*-scan measurements, i.e. measurements of the harmonic signal as a function of the position *z* of the focus of the driving laser with respect to the centre of the plasma in the direction of propagation, and with the distance of the propagation direction of the driving laser to the target surface (*x* coordinate).

Figure 4(a-c) shows the emitted TH and FH intensities in the metal plumes in the ns configuration, at 0.6 mm from the surface of the target, as functions of the time delay. The curves obtained were normalized for easier comparison. One temporal component is observed for all three metals. The highest up conversion yield is obtained at the

optimum phase matching conditions when the free-electron-induced dispersion is overcome by dispersion attributable to atoms, ions and other nonlinear species created in the ablation plume (see below). The optimal delays are listed in detail in Table 1, where it is noted that further away from the target, at a distance of 1 mm, the optimum delay is temporally displaced as expected, because the nonlinear emitters ejected from the target take longer to reach the plume region that interacts with the driving laser. It is also interesting to note that the relative strength of the third and fifth harmonics is independent of the time delay, indicating that this ratio is not governed by the instantaneous density of nonlinear plume species.[20] The different optimal delays and the widths of the time delay distributions, as displayed in Figure 4(a-c) among the three metals illustrate the diverse composition and dynamics of the ablation plume of each material.

As concerns the spatial behaviour of the harmonic signal generated by the ns beam across the plume, Figure 4(d) includes, as an example, the *z*-scan measurements performed for copper under the conditions marked with an arrow in Figure 4(b). The *z*-scan, presents a single maximum, corresponding to focusing the driving laser at the centre of the plasma and this characteristic is found also for Mn and Ag. Table 2 summarizes the obtained *z*-scans results obtained by fitting the data with Gaussian functions. A broader structure is observed for the TH beam as compared with the FH; this difference is attributable to the sharper driving laser intensity dependence of the FH signal and to the width of the plasma density profile along the propagation direction (about the Rayleigh length of the focused laser estimated in 2 mm). It is also found that the FWHM of the harmonic signals for Mn is larger than those corresponding to the other two metals. This indicates that for this lightest metal, the angular distribution of nonlinear species is spatially broader over the plane perpendicular to the normal to the

surface, i.e. they are emitted over an angularly wider distribution than in the case of Cu and Ag.

The dependence of the TH signal generated in the ps domain with the time delay between ablation and probe lasers was also measured for the three studied metals at 0.2 mm from the target. A representative result is shown in Figure 5(a) for the case of copper. Similar delay dependence is observed for Mn and Ag, and the times of maximum TH signal are listed in Table 1. It is important to note that, in striking contrast with the ns results (Figures 4(a-c)), the harmonic signal decays much faster with delay and vanishes after few tens of ns. Figure 5(b) displays the *z*-scan measurements performed on this material. The FWHM of the signal for copper is 14 mm, about a factor of 3 larger that the value obtained in the corresponding ns experiment. Values for Mn and Ag are also listed in Table 2. FWHM values derived from *z*-scan measurements in the ns and ps experiments were obtained by probing different plasma regions where efficient HG was observed, i.e. at 0.6 mm by the ns driving beam and closer to the target at 0.2 mm by the ps beam. The FWHM values (Table 2) serve to estimate the extension of nonlinear emitters along the region parallel to the target surface probed by the driving laser.

The measurements of the intensity of the harmonic signals as a function of the distance to the target *x* give additional information of the spatial dimensions of the laser-created nonlinear media (Figure 6). In Figure 6(a) the behaviour of the TH generated by ns IR laser is plotted for an ablation-driving delay that corresponds to maximum TH. It is observed that the harmonic signal is no longer visible for distances longer than 3 mm away from the target for all three materials. Figure 6(b) shows the corresponding results in the ps case, where it is found that at distances over 0.30 mm from the target the harmonic signal is negligible. The lesser extent of plume expansion in the direction

perpendicular to the target under ps ablation, as compared with the ns case, has been observed before in various materials.[21]

The dependence of harmonic signal with the distance to the target x is mediated by the corresponding dependence of the product $d\ ^2L_p\ ^2$, where d is the density and L_p is the length of nonlinear medium.[19] In an isotropic emission of nonlinear species from the target, d scales with x^{-2}. As L_p is expected to be proportional to x, the harmonic signal should be compatible with a x^{-2} dependence. The deviation in the ns experiments from the x^{-2} behaviour, indicated by a dotted line in Figure 6(a), is appreciable for Mn while Cu and Ag closely follow this dependence. A clear departure of the x^{-2} dependence is observed for all three metals in the ps experiments, Figure 6(b). It is expected that anisotropic plasma expansion, appearance of clusters in the plume or the presence of plasma electrons, at higher concentration in the ps plume due to the higher degree of ionization, would contribute to the observed x-dependence of harmonic signal.

The results outlined above allow discussing the identity and spatiotemporal distribution of the species contributing to frequency up conversion in the metal ablation plasmas. The position of the maxima found on the time delay dependence (Table 1, Figure 4) correspond to velocities of around 1.2×10^5-2.4×10^5 cm/s,. This range of velocities is typical for ejected species under these ns ablation conditions.[17,21] For ps experiments, the velocity of the nonlinear species derived from the delay dependence plots (Table 1, Figure 5) is around 10^6 cm/s.

Assuming a totally statistical ablation process, some insight can be obtained on the nature of nonlinear species contributing to HG in the ns ablation plasma.[17] Under the conditions of thermodynamic equilibrium in the first expansion stages, the same average kinetic energy is expected for all plasma components. Therefore it is possible to estimate the average size of species contributing to HG in the observed time delay range

if one considers that the atomic species are responsible for the early HG stage. For Mn, the temporal delay range of efficient HG, Figure 4(a), would correspond to the emission of species up to $(Mn)_{400}$. For copper and silver, the more restricted range of temporal delays for efficient HG, Figures 4(b,c), derives in a range of species up to about 60 atoms. For the ps laser ablation plasmas, the narrower delay range, of few tens of ns, for efficient harmonic generation provides an indication of the more homogeneous nature of the plasma species, both in terms of velocity and mass. Also in this case, the highest velocity of the ejected species anticipates a lower degree of interactions within the plume species, leading to lower clustering yield.

According to the above it should be expected that the nonlinear medium responsible for the observed HG, in both ns and ps ranges, is constituted, not only by metal atoms and ions but also by clustering species.[22] Cluster synthesis is often described as being carried out by laser ablation due to the rapid sample temperature increase, which favors plasma gas phase reactions.[17,23,24] Condensation of gaseous metal atoms to small clusters can be achieved by adiabatic cooling of the plume expanding in vacuum and reactive collisions within the plasma volume. Higher laser pulse energies lead to a higher density plasma and thus to a higher number of collisions between the ablated atoms, resulting in more efficient condensation and production of larger size clusters.

As regards the most versatile and efficient material for low-order harmonic generation of the fundamental 1064 nm radiation using the investigated ablation plasmas, the results presented here indicate that the ns plume of manganese can sustain HG in a large spatiotemporal plasma region and in a wide range of ablation energies. Earlier studies of HHG in the laser ablation plasma of this medium have demonstrated an extremely high harmonic cutoff with generation of up to the 101st harmonic.[15] On the other hand, upon ps ablation, the active temporal and spatial regions of the plume are very much

restricted with respect to ns ablation confined to few tens of ns after the ablation event and few hundred of micrometers close to the target. In both ns and ps cases, these results give insight on the nature of the nonlinear emitters responsible for HG, although more definitive conclusions will be drawn by studies in progress to characterize the cluster and nanoparticle content of the metal ablation plumes by time-of-flight mass spectrometry and by analysis of the plume material deposited on a substrate placed in the proximity of the target.[25,26]

IV CONCLUSIONS

Low-order harmonic generation from laser ablation plasmas of the metals manganese, copper and silver, produced by 1064 nm pulses of duration in the range of ns and ps, have been generated with a driving fundamental beam with pulses of the same duration as those used for ablation. In both cases, it is observed that the temporal delay between ablation and driving laser which results in optimal HG is sensitive to the target properties. This is expected, as density, mechanical and thermal constants will have an influence on the heating of the target and the subsequent plasma expansion and cooling, and therefore on the distribution of masses and velocities of plasma species. The results also show that the duration of the ablating pulse determines to a large extent the temporal and spatial regions of the plume at which efficient low-order harmonic generation can be achieved. It is observed that the ns ablation plume provides a broad spatiotemporal range where efficient low-order HG can be achieved.

ACKNOWLEDGEMENTS

Funding has been provided by Ministry of Science and Innovation of Spain (MICINN) under Project CTQ2010-15680. M. L.-A. thanks CSIC for a JAE-Pre contract. M.O. and

M.S. acknowledge CONSOLIDER CSD2007-00058 and CAM (Geomateriales P2009/MAT 1629) respectively for contracts. R.A.G., G.S.B., N.K.S., R.I.T. and T.U. thank the Academy of Sciences for the Developing World (TWAS) for partial support of these studies (TWAS Research Grant 09-113 RG/PHYS/AS G). Useful discussions with Dr. R. de Nalda are gratefully acknowledged.

REFERENCES

1 C.Y. Ng, *Ann. Rev. Phys. Chem.* **53**, 101 (2002).

2 A.H. Zanganeh, J. H. Fillion, J. Ruiz, M. Castillejo, J. L. Lemaire, N. Shafizadeh, and F. Rostas, *J. Chem. Phys.* **112**, 5660 (2000).

3 J.J. Macklin, J.D. Kmetec, and C.L. Gordon, *Phys. Rev. Lett.* **70**, 766 (1993).

4 X.F. Li, A. L'Huillier, M. Ferray, L.A. Lompre, and G. Mainfray, *Phys. Rev. A* **39**, 5751 (1989).

5 C. Spielmann, N.H. Burnett, S. Sartania, R. Koppitsch, M. Schnurer, C. Kan, M. Lenzner, P. Wobrauschek, and F. Krausz, *Science* **278**, 661 (1997).

6 N. Hay, R. de Nalda, T. Halfmann, K.J. Mendham, M.B. Mason, M. Castillejo, and J.P. Marangos, *Eur. Phys. J. D* **14**, 231 (2001).

7 N. Hay, R. Velotta, M.B. Mason, M. Castillejo, and J.P. Marangos, *J. Phys. B: At. Mol. Opt. Phys.* **35**, 1051 (2002).

8 S.M. Gladkov, and N. I. Koroteev, *Sov. Phys. Usp*. **33**, 554 (1990).

9 Y. Akiyama, K. Midorikawa, Y. Matsunawa, Y. Nagata, M. Obara, H. Tashiro, and K. Toyoda, *Phys. Rev. Lett.* **69**, 2176 (1992).

10 S. Kubodera, Y. Nagata, Y. Akiyama, K. Midorikawa, M. Obara, H. Tashiro, and K. Toyoda, *Phys. Rev. A* **48**, 4576 (1993).

11 C.-G. Wahlström, S. Borgström, J. Larsson, and S.-G. Pettersson, *Phys. Rev. A* **51**, 585 (1995).

12 R. A. Ganeev, V. I. Redkorechev, and T. Usmanov, *Opt. Commun.* **135,** 251 (1997).

13 R.A. Ganeev, M. Suzuki, M. Baba, H. Kuroda, and T. Ozaki, *Opt. Lett*. **30**, 768 (2005).

14 R. A. Ganeev, M. Suzuki, T. Ozaki, M. Baba, and H. Kuroda, *Opt. Lett*. **31**, 1699 (2006).

15 R.A. Ganeev, *J. Phys. B* **40**, R213 (2007).

16 M. Oujja, R. de Nalda, M. López-Arias, R. Torres, J.P. Marangos, and M. Castillejo, *Phys. Rev. A* **81**, 043841 (2010).

17 R. de Nalda, M. López-Arias, M. Sanz, M. Oujja, and M. Castillejo, *Phys. Chem. Chem. Phys.* **13**, 10755 (2011).

18 R.A. Ganeev, G.S. Boltaev, R.I. Tugushev, T. Usmanov, M. Baba, and H. Kuroda, *J. Opt.* 12 (2010) 055202.

19 J.F. Reintjes, *Nonlinear Optical Parametric Processes in Liquids and Gases*, Academic Press, Orlando, 1984.

20 W. Theobald, C. Wülker, F. P. Schäfer, and B. N. Chichkov, *Optics Comm.* **120**, 177 (1995).

21 F. Claeyssens, M.N.R. Ashfold, E. Sofoulakis, C.G. Ristoscu, D. Anglos, and C. Fotakis, *J. Appl. Phys.* **91**, 6162 (2002).

22 M. B. Knickelbein, *Phys. Rev. Lett.* **70**, 014424 (2004).

23 H. Lillich, J. Wolfrum, V. Zumbach, L. E. Aleandri, D. J. Jones, J. Roziere, P. Albers, K. Seibold, and A. Freund, *J. Phys. Chem.* **99**, 12413 (1995).

24 U. Chakravarty, P. A. Naik, C. Mukherjee, S. R. Kumbhare, and P.D. Gupta, *J. Appl. Phys.* **108**, 053107 (2010).

25 M. Sanz, M. López-Arias, J. F. Marco, R. de Nalda, S. Amoruso, G. Ausanio, S. Lettieri, R. Bruzzese, X. Wang, and M. Castillejo, *J. Phys. Chem. C*, **115**, 3203 (2011).

26 M. Sanz, R. de Nalda, J. F. Marco, J. G. Izquierdo, L. Bañares, and M. Castillejo, *J. Phys. Chem. C* **114**, 4864 (2010).

Table 1. Position in ns of the temporal maximum of TH and FH in 1064 nm ablation plasmas of metals in ns and ps domains.

	Mn		Cu		Ag	
Distance (mm)	0.6	1.0	0.6	1.0	0.6	1.0
TH (ns)	500	600	250	300	400	450
2FH (ns)	500	600	250	300	400	450
Distance (mm)	0.2					
TH (ps)	28		20		30	

Table 2. Full-width-half maximum of harmonic emissions (in mm) as a function of the position of IR driving laser focus with respect to centre of ablation plasma in the direction of laser propagation (*z*-scan). The distance of the propagation direction of the driving laser to the target is 0.6 mm for ns pulses and 0. 2 mm for ps pulses. Estimated error is 5%.

	Mn	Cu	Ag
TH (ns)	8	5	5
2FH (ns)	5	3	4
TH (ps)	17	14	7

Figure captions

FIG. 1. Spectra of emissions detected (a) upon ablation of a copper target with 6 ns, 1064 nm pulses of 11 mJ, and in the presence (b) of the fundamental driving beam of the same wavelength propagating at 0.6 mm from the target with a delay of 250 ns. The energy of the driving beam was 560 mJ. The lines corresponding to third harmonic (TH) and the second order of the fifth harmonic (2FH) and of the atomic copper lines are indicated.

FIG. 2. Normalized intensity of the third harmonic (355 nm) of the ns driving laser as function of the ablation pulse energy for (a) Mn, (b) Cu and (c) Ag. The conditions were the following: driving laser energy 560 mJ, distance to target 0.6 mm, delay 250 ns. Both ablation and driving laser pulses have durations within ns range.

FIG. 3. (Color on line) Log-log plot of the signals corresponding to the TH (open circles) and of the second order of the FH (2FH, solid circles) of the ns driving laser detected at a distance of 0.6 mm from the target as function of the laser pulse energy, for ns, 1064 nm ablation of metal targets. The conditions were (a) Mn, ablation pulse energy 5 mJ, delay 250 ns; (b) Cu ablation pulse energy 10 mJ, delay 250 ns; and (c) Ag ablation pulse energy 12 mJ, delay 300 ns. The units in the vertical axes allow the comparison of the relative intensity of the same harmonic for the three metals. As indicated, the slopes are compatible with a third and fifth order non-linear processes.

FIG. 4. (Color on line) Normalized harmonic signals of the third (open circles) and fifth (solid circles) orders of the IR ns driving laser in metal ablation plasmas induced by a 6 ns, 1064 nm ablation laser with pulse energy of 5, 10 and 12 mJ for (a) Mn, (b) Cu and (c) Ag respectively, as a function of the delay between the ablation event and the arrival of the ns driving laser, and at a distance of 0.6 mm from the surface of the target. The

driving laser power was 560 mJ. A *z*-scan plot for copper, where the TH and FH are measured as a function of the position of the IR focus (*z*) with respect to the centre of the ablation plasma in the direction of propagation, is represented in (d) for a delay of 250 ns. Experimental points are shown together with Gaussian fits with the widths (FWHM) indicated in the graph.

FIG. 5. Third harmonic (a) of the IR ps driving laser in copper ablation plasma induced by a 38 ps, 1064 nm ablation laser with pulse energy of 10 mJ as a function of the delay between the ablation event and the arrival of the ns driving laser, and at a distance of 0.2 mm from the surface of the target. The driving laser power was 4.5×10^{13} W/cm^2. Z-scan plot (b) for copper, where the TH is measured as a function of the position of the IR focus (*z*) with respect to the centre of the ablation plasma in the direction of propagation, for a delay of 25 ns. The experimental points are shown together with the gaussian fit yielding the indicated width (FWHM).

FIG. 6. (Color on line) Normalized intensity of the TH signal at 355 nm as the position of the fundamental IR beam is displaced from the surface of the metal target (*x* distance) with ablation and driving lasers with pulses of (a) ns and (b) ps duration. For each distance probed, the delay between the ablation beam at 1064 nm and the fundamental beam was set at the value corresponding to the optimum signal. The solid lines are visual guides while the dotted lines represent a x^{-2} decay.

Figure 1

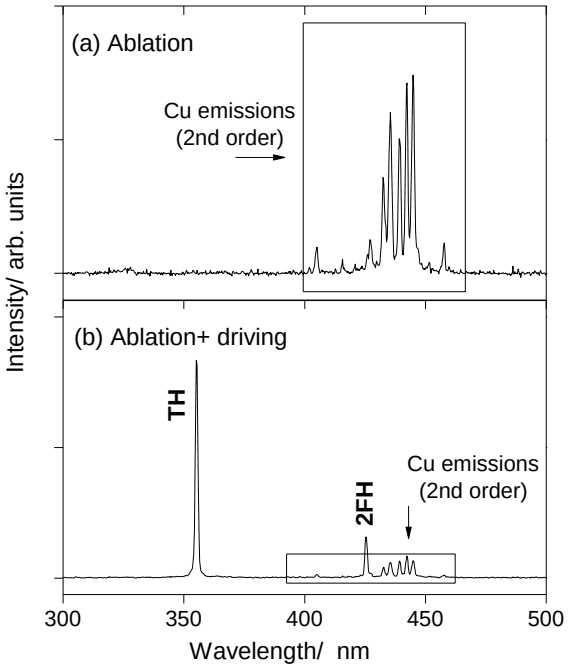
(a) Ablation
Cu emissions
(2nd order)
(b) Ablation+ driving
TH
2FH
Cu emissions
(2nd order)
Intensity/ arb. units
300
350
400
450
500
Wavelength/ nm

Figure 2

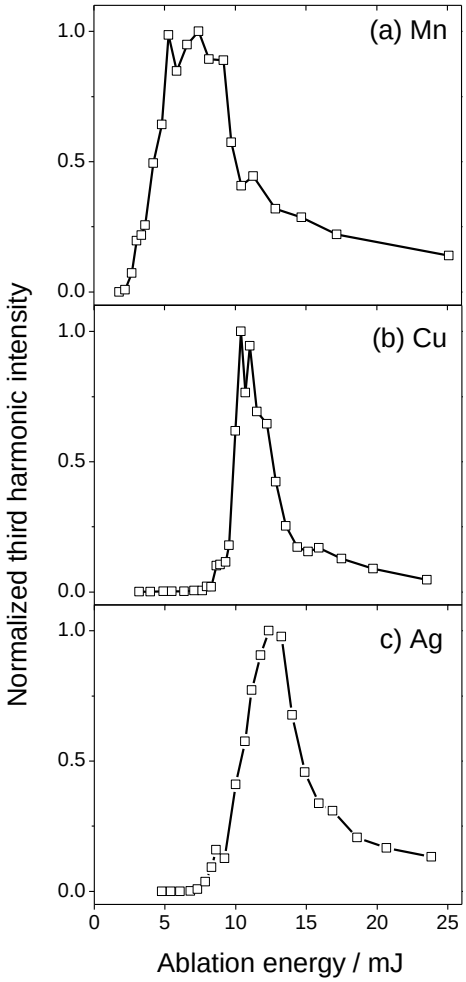
(a) Mn
(b) Cu
c) Ag
Normalized third harmonic intensity
Ablation energy / mJ
1.0
0.5
0.0
0
5
10
15
20
25

Figure 3

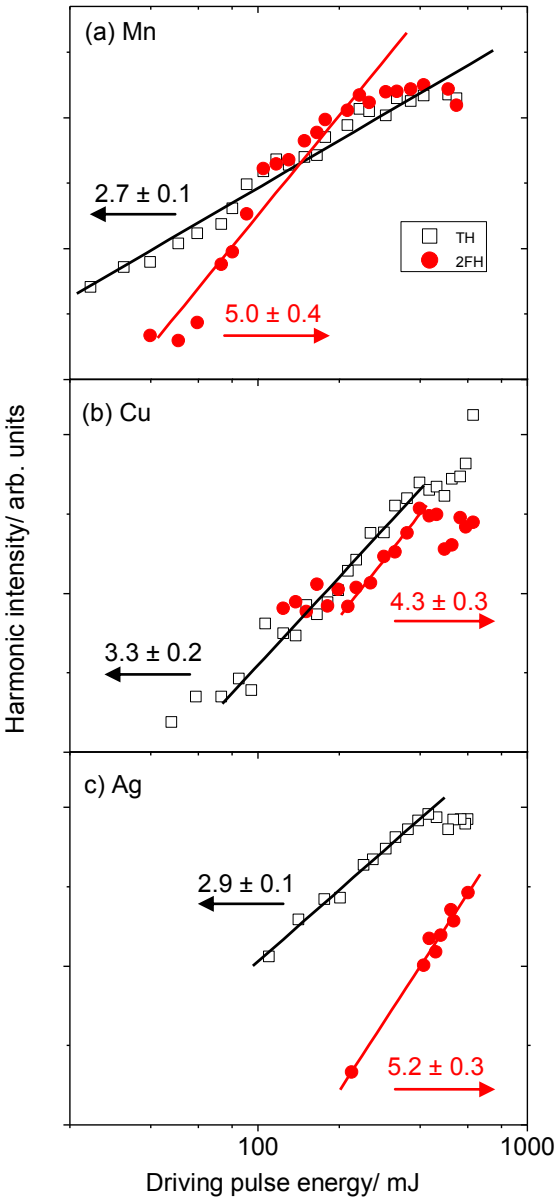
(a) Mn
2.7 ± 0.1
TH
2FH
5.0 ± 0.4
(b) Cu
4.3 ± 0.3
3.3 ± 0.2
c) Ag
2.9 ± 0.1
5.2 ± 0.3
Harmonic intensity/ arb. units
100
1000
Driving pulse energy/ mJ

Figure 4

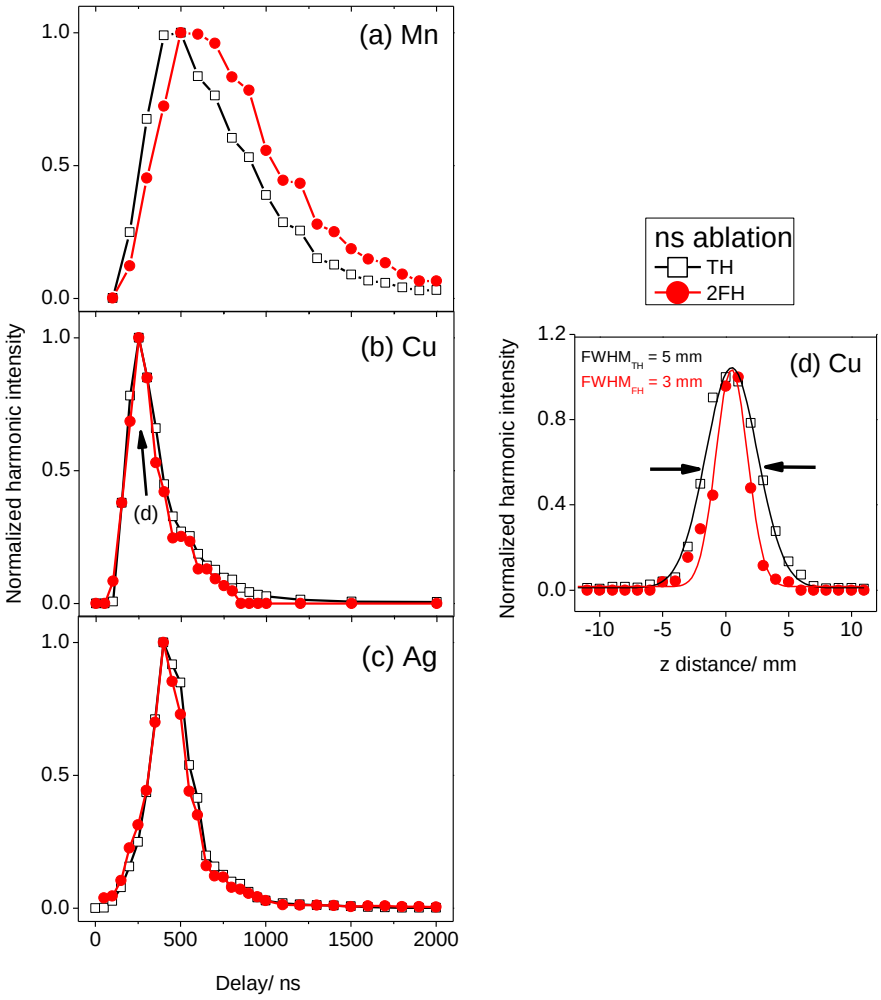
(a) Mn
(b) Cu
(c) Ag
(d)
Normalized harmonic intensity
Delay/ ns
ns ablation
TH
2FH
(d) Cu
FWHM$_{TH}$ = 5 mm
FWHM$_{FH}$ = 3 mm
Normalized harmonic intensity
z distance/ mm

Figure 5

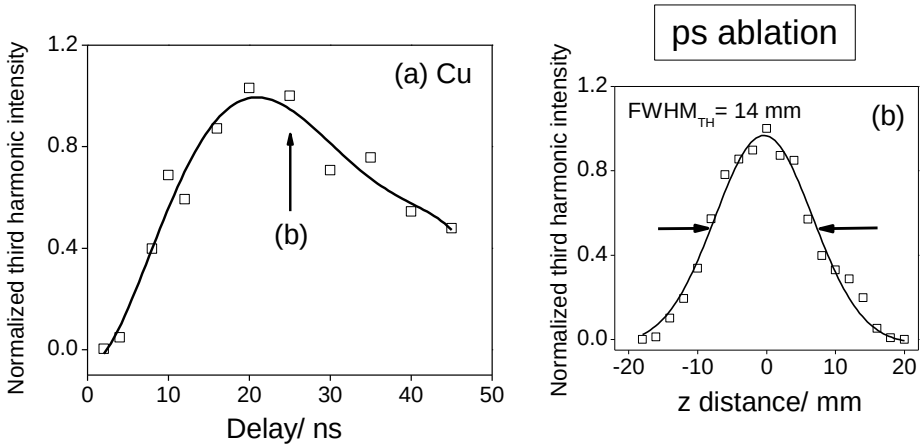

Figure 5

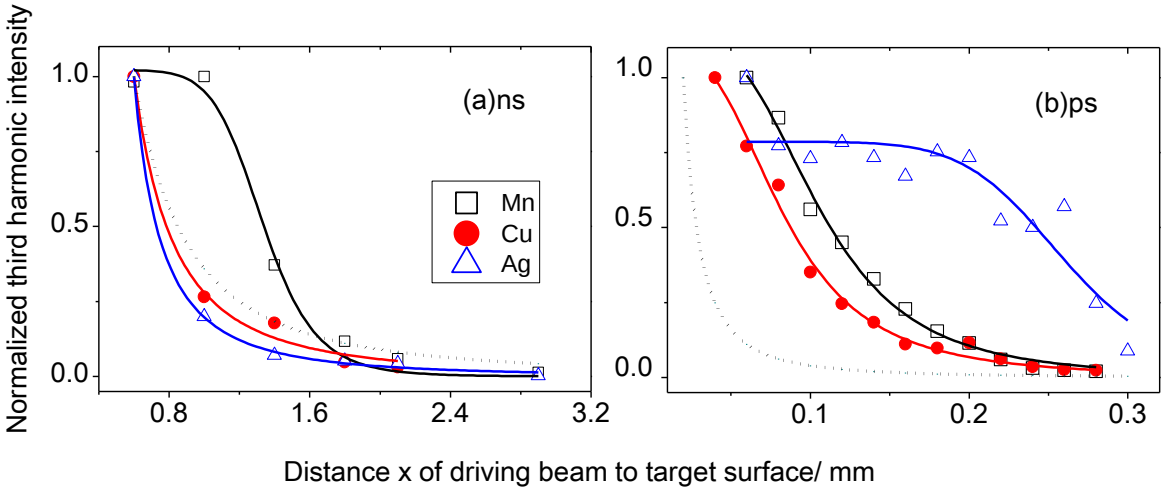
Normalized third harmonic intensity
1.0
0.5
0.0
(a)ns
Mn
Cu
Ag
0.8
1.6
2.4
3.2
(b)ps
0.1
0.2
0.3
Distance x of driving beam to target surface/ mm

Figure 6